Annu. Rev. Earth Planet. Sci. 2003. 31:303–28
doi: 10.1146/annurev.earth.31.091602.113555

First published online as a Review in Advance on February 10, 2003

GLOBAL MANTLE TOMOGRAPHY: Progress Status in the Past 10 Years

Barbara Romanowicz
Seismological Laboratory, University of California, Berkeley, California 94720; email: barbara@seismo.berkeley.edu

Key Words seismic structure, imaging, Earth interior

■ **Abstract** We review the present status of global mantle tomography and discuss two main classes of models that have been developed in the past 10 years: P velocity models based on large datasets of travel times from the International Seismological Centre bulletins, often referred to as "high resolution" models, and S velocity models based on a combination of surface wave and hand picked body wave travel times, or waveforms, referred to as "long wavelength" models. We discuss their respective strengths and weaknesses, as well as progress in the resolution of other physical parameters, such as anisotropy, anelasticity, density, and bulk sound velocity using tomographic approaches. We present the view that future improvements in global seismic tomography require the utilization of the rich information contained in complete broadband seismic waveforms. This is presently within our reach owing to theoretical progress as well as the increase in computational power in recent years.

INTRODUCTION

Global seismic tomography of Earth's mantle is a powerful tool for the investigation of the dynamics of Earth's interior. When combined with geodynamical simulations and mineral physics experiments that help in their interpretation, tomographic images allow us to address the following outstanding questions: What is the fate of lithospheric slabs as they descend into the deep mantle? What is the morphology and significance of rising plumes, and in what regions of the mantle do they originate? Are there distinct geochemical reservoirs in the mantle? What is the scale and nature of heterogeneity in the boundary layer at the base of the mantle? Geophysicists are still debating these and other fundamental questions (e.g., Albarède & van der Hilst 1999), whereas seismologists strive to improve the lateral and depth resolution of their tomographic models.

There has been much progress in seismic tomography since its introduction in the late 1970s (e.g., Aki et al. 1977, Sengupta & Toksöz 1977, Dziewonski et al. 1977). The first global models were able to resolve only the largest wavelengths (∼3000–5000 km) through parameterizations in terms of spherical harmonics up

to degree 6–8. They also focused separately on the lower mantle, using P wave travel time data (e.g., Dziewonski et al. 1977, Dziewonski 1984), or on the upper mantle, using surface wave dispersion data (e.g., Woodhouse & Dziewonski 1984, Nataf et al. 1986). In parallel, many regional tomographic studies of the upper mantle were conducted, focusing either on subduction zones, which correspond to a favorable geometry for P travel time tomography (e.g., Kamiya et al. 1988, van der Hilst & Spakman 1989) or oceanic areas largely inaccessible to body waves but well sampled by surface waves (e.g., Montagner 1986). A review of mantle tomography of the 1980s can be found in Romanowicz (1991) and one of tomographic S velocity models of the early 1990s in Ritzwoller & Lavely (1995). Here, we mostly focus on more recent work.

The last decade has seen a spectacular increase in the number of regions studied by tomographic methods. However, we restrict our review to global studies. Global 3-D models now span the entire depth range of the mantle and achieve lateral resolutions corresponding to wavelengths of less than 1000 km, and in some places, 500 km. In addition to solving for volumetric heterogeneity, tomographers are also starting to investigate other types of seismologically derived information, such as lateral variations in anisotropy, attenuation, density, and in the topography of upper mantle discontinuities, as well as the relation between P and S velocity distributions.

Two rather distinct approaches have prevailed in global tomography in the past 10 years: most global P wave velocity (V_p) models are based on a local parameterization and use the reports from the ISC (International Seismic Center) bulletins as a database. We call these high resolution models because, as we see later, they can locally achieve lateral resolution of a few hundred kilometers or less. On the other hand, most global models of S wave velocity (V_s) are based on a global polynomial parameterization and collections of seismic travel times and/or waveforms that have been individually collected from the growing global ensemble of digital broadband seismic stations. We refer to those as long wavelength models. We first discuss the respective strengths and weaknesses of these two classes of models and then discuss progress in the retrieval of other physical parameters. Finally, we describe recent theoretical progress and offer our perspective on how this can help us move forward toward the next generation of waveform based, finer-scale, global models.

HIGH RESOLUTION MODELS

Most P velocity models to date have been based on the extensive dataset of first arrival travel time picks provided over the past 30 years in the bulletins of the ISC. In using this dataset, the large quantity of global data available (hundreds of thousands to millions of travel time picks) compensates for the absence of control on the quality of individual picks. The tomographic mantle models thus derived (e.g., Zhou 1996, 2001; van der Hilst et al. 1997; Obayashii & Fukao

1997; Vasco & Johnson 1998; Bijwaard et al. 1998; Kennett et al. 1998; Boschi & Dziewonski 2000; Karason & van der Hilst 2001) are parameterized in local basis functions, typically cells of size 1 to 3^o in the upper mantle, and 3 to 5^o in the lower mantle. Zhao (2001) uses a grid parameterization, better suited for 3-D ray tracing. Data processing generally involves earthquake relocation, station corrections, and the construction of summary rays. The more recent models use the ISC data reprocessed by Engdahl et al. (1998) (the so-called EHB catalog), which has involved the reidentification of phases and the relocation of hypocenters.

From the theoretical point of view, these tomographic inversions are performed in the framework of ray theory. Because of the large number of data and parameters, they employ iterative approximative techniques, such as LSQR or SIRT (e.g., Paige & Saunders 1982, Spakman & Nolet 1988), that take advantage of the sparseness of the matrices involved. However, the approximations involved do not result in a strong bias in the tomographic models produced (e.g., Boschi & Dziewonski 1999).

Because of the particular distribution of sources (concentrated around subduction zones) and stations (mostly on continents), these inversions, dominated by first arrival *P* travel time data, provide good resolution under subduction zones but lack coverage under the oceans, both in the upper mantle and in the lower mantle. In order to improve resolution in the oceans, it is necessary to add later-arriving phases that are not as frequently and reliably reported to the ISC. Different authors have added a combination of other phases to *P*. For example, Bijwaard et al. (1998) included arrival times of the depth phases *pP* and *pwP*, whereas Obayashi & Fukao (1997) used *PcP* and investigated mantle volumetric structure as well as structure at the core-mantle boundary (CMB). Boschi & Dziewonski (2000) also used *PcP* as well as reports of core-phases PKP_{df} and PKP_{bc}, which, in addition to the CMB, allowed them to investigate trade-offs between mantle structure and structure in the core. Karason & van der Hilst (2001) used *P*; *pP*; *pwP*; reports of core phases, as well as a dataset of hand-picked differential $PKP_{ab} - PKP_{df}$ and $PKP_{ab} - PKP_{bc}$ travel times, and most significantly, a small dataset of $PKP - P_{diff}$ travel times obtained by waveform cross-correlation, which allowed them to improve resolution in the low velocity region at the base of the mantle under the central Pacific Ocean. Vasco & Johnson (1998) used exclusively bulletin data, but included *PcP*, PKP_{ab}, and PKP_{df}. These authors also assembled a dataset of V_s sensitive phases from ISC bulletins: *S*, *SS*, and *ScS*, and obtained a V_s model as well as a V_p model. Still, many areas of the ocean (both spatially and in depth) remain unsampled or poorly resolved (Figure 1). Therefore, these models tell us little about the low velocity regions in the mantle, which are preferentially located under the oceans. In particular, this leads to controversies, yet unresolved, such as that concerning the depth extent of plumes that underlie hot spots, such as Iceland (e.g., Bijwaard & Spakman 1999, Foulger et al. 2000, Zhao 2001).

On the other hand, these models have provided us with sharp images of fast velocity slabs under the western Pacific and the Americas, and they have clarified

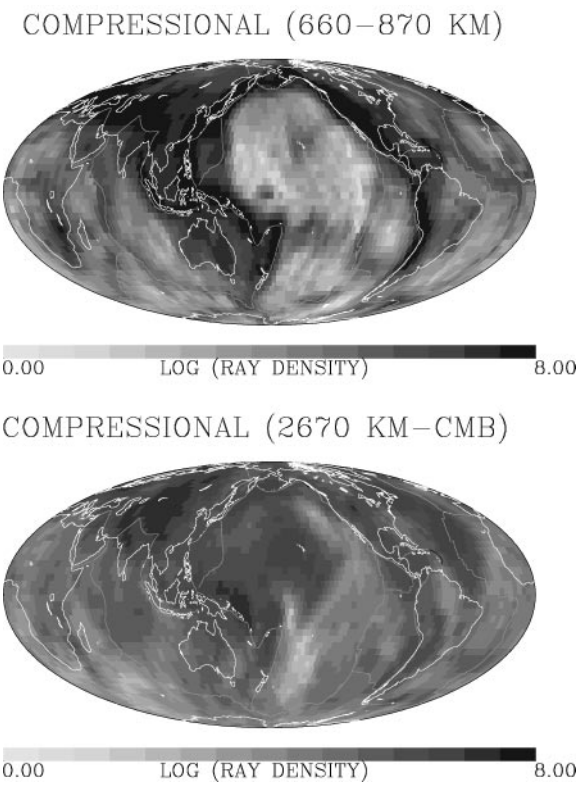

Figure 1 Examples of coverage obtained at different depths in the mantle using compressional wave phases from the ISC, for the time period 1964–1987 (Vasco & Johnson 1998). The phases included are P, PP, PKPab, PKPbc, PKPdf. The gray scale indicates the logarithm of the number of summary rays intersecting the cells in the given layers. The cells are equal area, equivalent to 6deg by 6deg at the equator.

the interaction of these slabs with the mantle transition zone, in particular, the 670-km discontinuity (Figure 2). Some slabs lie flat and do not penetrate far into the lower mantle, whereas others appear to continue to great depths (e.g., van der Hilst et al. 1997). In particular, these models clearly show linear zones of fast velocities at depths between 900–1300 km under southeast Asia and north and central America, which are thought to be associated with ancient subduction of the Tethys and Farallon plates, respectively (Figure 2). Therefore, the high-resolution P models of the 1990s have now established that the 670-km discontinuity is at most a partial barrier to global circulation. Recently, Fukao et al. (2001) have suggested that the barrier to slab penetration into the lower mantle is not at the 670-km discontinuity, but rather at the bottom of the transition zone, as defined by Bullen (1963), around a depth of 1000 km. Other studies suggest

that coherent structure related to slabs reaches at least 1700 km (van der Hilst & Karason 1999).

Deeper in the mantle, as already mentioned, resolution is poorer in the middle of the oceans than under subduction zones. Nevertheless, most models show some striking common features in D″ (Figure 3): most prominently, high velocities under eastern Asia and central America and a band of high velocities at mid-northern latitudes across the Pacific ocean. This is also seen in a D″ model derived from hand-picked $PKP(AB-DF)$ and $PcP-P$ data by Tkalčić et al. (2002).

As for CMB topography derived from these tomographic studies, there is not yet a consensus on even the longest wavelengths, an issue already debated in the 1980s (e.g., Creager & Jordan 1986, Morelli & Dziewonski 1987, Doornbos & Hilton 1989). In particular, there appears to be an incompatibility between results obtained using *PcP* mantle phases and *PKP* core phases. This could be due to poor resolution (e.g., Rodgers & Wahr 1993, Stark & Hengartner 1993) or some not yet well-understood effect, in particular trade-offs between CMB topography and structure in D″ (e.g., Sylvander & Souriau 1996). Using *PcP*, the maps obtained by Obayashi & Fukao (1997) show a strong zonal degree 2 component, also present in the model of Rodgers & Wahr (1993), but not in that of Boschi & Dziewonski (2000). On the other hand, all three models show depressed CMB roughly under the location of subduction zones in the western Pacific and under central America.

Finally, both Vasco & Johnson (1998) and Boschi & Dziewonski (2000) have discussed trade-offs between mantle structure (and anisotropy, in the latter case) and outer core structure in inversions that include core phases. Both have concluded that trade-offs are weak; however, the outer core structures that they obtain are very different and therefore encounter skepticism, given the generally accepted viewpoint that the outer core should be well mixed (Stevenson 1987).

LONG WAVELENGTH MODELS

The second type of global tomographic models primarily concern S velocity (V_s) structure (although some V_p models have also been derived with similar techniques and geometry, e.g., Masters et al. 2000). These models rely primarily on data collected by individual scientists from global databases of long period and broadband seismic waveforms collected by members of the Federation of Global Seismic Networks (FDSN). Varying from author to author, the data considered include normal mode spectral measurements (Resovsky & Ritzwoller 1999a, Masters et al. 1996), which provide constraints on the longest wavelengths of the part of lateral heterogeneity that is symmetric with respect to Earth's center, and surface wave dispersion or waveform data, which provide sampling in the upper mantle, in particular across the oceans. Grand et al. (1997) and Grand (2002) constrain the upper mantle by use of upper mantle triplication phases (Grand 1994). To attain resolution in the lower mantle, travel times of *S*, *SS*, *SSS*, *ScS*, ScS_n, and *SKS* are

generally measured using cross correlation techniques; this includes differential travel times as well as absolute travel times, the latter measured by comparison with synthetic seismograms computed in spherically symmetric Earth models, accounting for Earth's ellipticity (Masters et al. 1996, Su et al. 1994, Grand et al. 1997, Liu & Dziewonski 1998, Ritsema et al. 1999, Gu & Dziewonski 2002). Some groups also use long period waveforms of body waves using different theoretical frameworks, as is discussed later (Su et al. 1994, Liu & Dziewonski 1998, Gu et al. 2001, Li & Romanowicz 1996, Mégnin & Romanowicz 2000).

These whole-mantle inversions use a parameterization of the mantle in global basis functions in the horizontal dimension (spherical harmonics) and a polynomial or cubic spline representation in depth. For the first time, an inversion with a local parameterization in the horizontal direction, using spherical splines (e.g., Wang & Dahlen 1995) was presented in Gu et al. (2001). Chiao & Kuo (2001) have shown how to better deal with nonuniform sampling, through the use of a regularization scheme based on the actual ray-sampling of the mantle.

An issue that needs to be addressed when constructing models that utilize surface wave data is that of correcting for crustal structure. Indeed, lateral variations of V_s in the crust are very strong and influence the dispersion of surface waves even at the long periods (at least 60 s, more commonly 80 s) generally considered in global mantle inversions. Initially, simple models reflecting the zeroth order effects of crustal thickness variations between oceans and continents were used. Recently, two models of the crust have been proposed that regionalize crustal structure based on compilations of regional refraction and reflection surveys (CRUST5.1; Mooney et al. 1998) or a priori knowledge on crustal and uppermost mantle parameters consistent with various geophysical data (3SMAC; Nataf & Ricard 1996). An adequate model of the crust is only the first step in the crustal correction process because lateral variations in Moho depth can exceed 50% over horizontal scales of less than 1000 km; it has been pointed out that the problem is strongly nonlinear and that standard perturbation theory is inadequate to compute these corrections. Montagner & Tanimoto (1991) propose a more rigorous approach by computing perturbations regionally, using average oceanic and continental models separately. In addition to a-priori crustal corrections, Li & Romanowicz (1996) allow the Moho depth to vary as a free parameter in their tomographic inversion. Boschi & Ekström (2002) use sensitivity kernels computed point by point over Earth based on crustal structure at each location, and show that such an approach has a noticeable effect on the amplitudes of lateral variations of upper-mantle structure retrieved.

Because of the sampling provided by surface waves and multiple bouncing body waves included in the inversions, the "long-wavelength" S models have the advantage of allowing good constraints on the longest wavelength features (i.e., the lowest spherical harmonic degrees) of mantle heterogeneity at the global scale, and in particular, better resolution in the oceans. Gradually refined since the mid-1980s, at which time the maximum degree of spherical harmonics expansion was 6–8, models are now displaying details corresponding to spherical

harmonics degree 24 or larger (i.e., spatial resolution of under 1000 km at the surface). They have confirmed or revealed several distinctive and stable large-scale features of mantle structure that provide strong constraints on mantle circulation models. First, the spectrum of lateral heterogeneity varies with depth in the mantle (Figure 4). Dominated by low degrees (up to degree 8) in the uppermost mantle and by degree 2 in the transition zone (e.g., Gu et al. 2001, Li & Romanowicz 1996), the spectrum becomes approximately white at midmantle depths, before changing again to a red character, dominated by degrees 2 and 3, in the lowermost

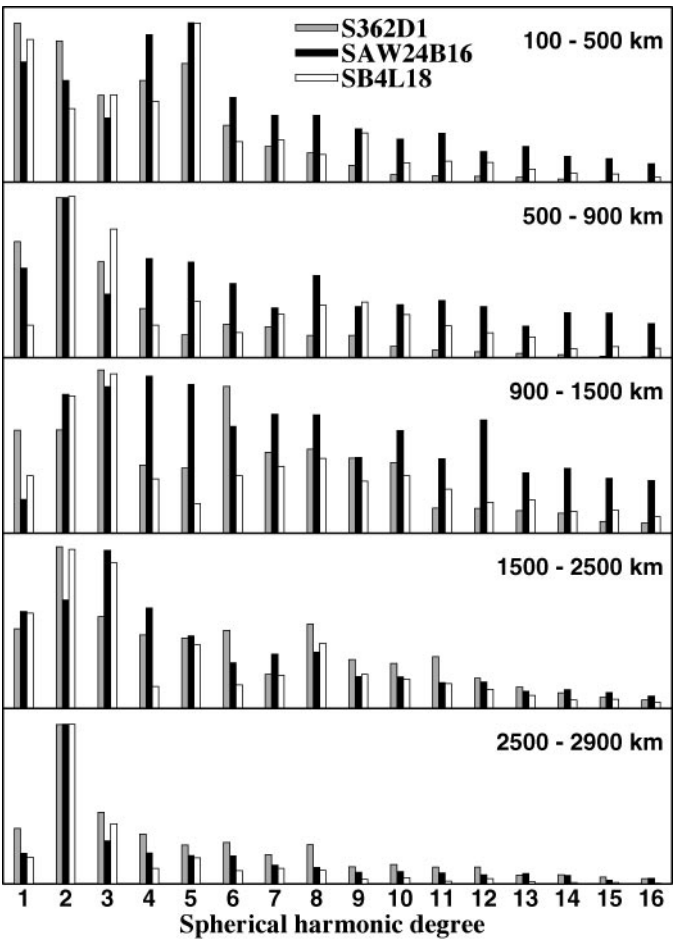

Figure 4 Comparison of spectra of S heterogeneity in different depth ranges, for degrees 1–16, for three recent models: SAW24B16 (Mégnin & Romanowicz 2000), SB4L18 (Masters et al. 2000), and S362D1 (Gu et al. 2001). In each depth range, the spectra have been normalized to the largest term.

$\sim$ 400 km of the mantle (Figure 4). The rms heterogeneity follows these changes, being strong in the topmost mantle, weak in the mid-mantle, and increasing again at the base of the mantle (Figure 5). S velocity structure is correlated with tectonics in the first 200–300 km of the upper mantle, with low velocities associated with mid-ocean ridges and back arcs, and fast velocities in continental shield and platform areas (Figure 6). S velocity gradually increases as a function of age in the oceans. In the transition zone (400–1200 km), the patterns are most clearly dominated by fast velocities associated with subduction

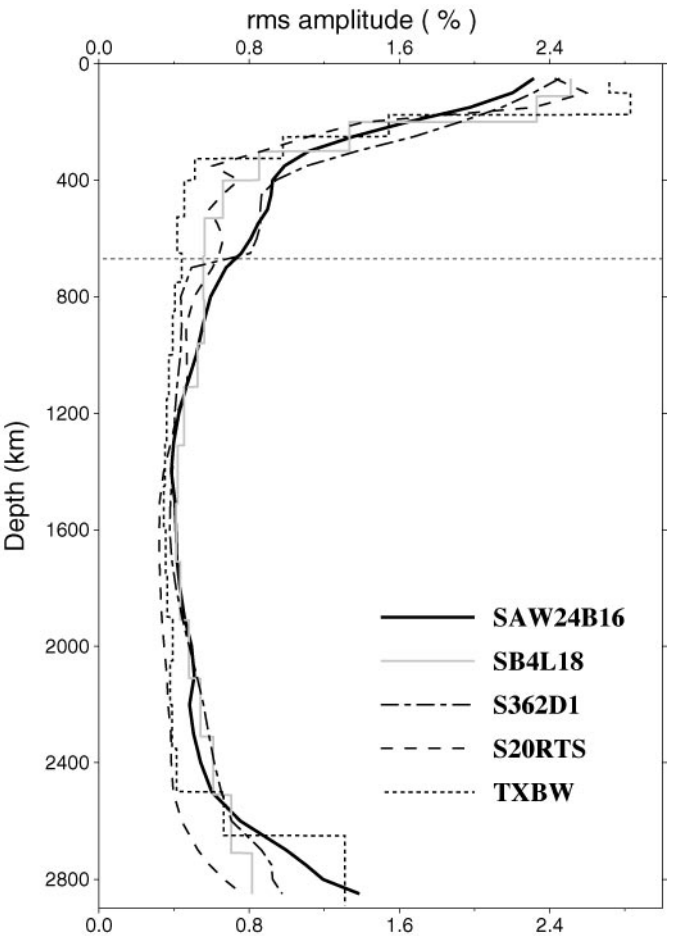

Figure 5 Comparison of rms S velocity variation with depth for four recent global tomographic models of the mantle: SAW24B16 (Mégnin & Romanowicz 2000), SB4L18 (Masters et al. 2000), S362D1 (Gu et al. 2001), S20RTS (Ritsema et al. 1999), and TXBW (Grand 2002).

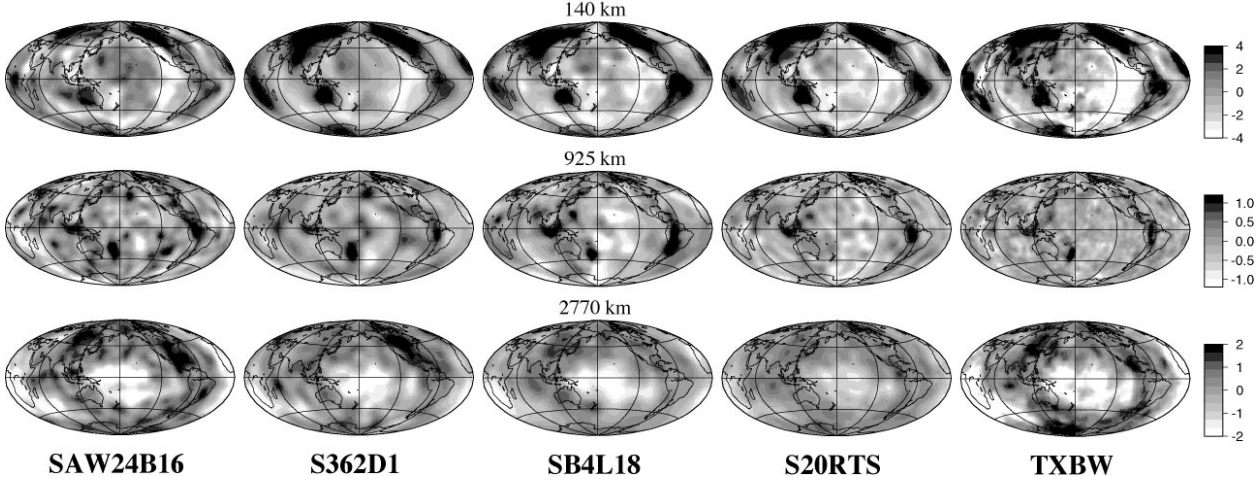

Figure 6 Comparison of maps of lateral variations in S velocity at three sample depths in the upper, mid, and lowermost mantle, for the same five recent models as shown in Figure 4.

zones, whereas between 1200 and 2000 km, it is more difficult to recognize any coherent patterns. Toward the bottom of the mantle, the structure becomes more organized again (Figure 6) and reveals two distinctive large low-velocity regions, generally referred to as superplumes, under the central Pacific and under Africa. The central Pacific low velocity region is surrounded by a ring of fast velocities, commonly associated with fossil subduction. A more detailed review of the structure in D″ derived from tomographic and other studies can be found in Garnero (2000).

All current models show many compatible features at long wavelengths, even though details vary significantly from one to the other (Figure 6). Correlation between models is very strong, at least up to degree 4 throughout the mantle.

When comparing these long wavelength models to the "high-resolution" P models discussed previously, it is encouraging to note that in most subduction zone areas they are very compatible, the former providing a "low-pass filtered" image of the latter, as recently illustrated by Fukao et al. (2001) (Figure 7).

The long wavelength models do not yet attain images in subduction zones that are as "crisp" as those of high-resolution P models. On the other hand, they provide better resolution in regions of low velocity under the oceans and, in particular, in the two "superplume" regions in the lowermost mantle. Although there are still many issues to be resolved regarding the nature and role of these superplumes in the general mantle circulation, it is clear from a comparison of different models (Figure 8), that they represent major features that rise high above the CMB, possibly connecting with low velocity structures in the upper mantle (e.g., Romanowicz & Gung 2002).

In addition to tomographic models that describe elastic velocity variations as a function of depth, many studies have been devoted to the global analysis of long period surface wave dispersion, often a first step in tomographic inversions for upper mantle structure, obtaining maps of phase velocities of Love and Rayleigh waves at different periods (typically 80–300 s). These maps (e.g., Zhang & Tanimoto 1993, Laske & Masters 1996, Trampert & Woodhouse 1996, Zhang & Lay 1996, Ekström et al. 1997) share many of the features already discussed for upper mantle structure, in particular, the correlation with tectonics of structure in the first 250 km. It is worth noting that Laske & Masters (1996) include amplitude and polarization constraints, which help resolve smaller-scale lateral variations of structure.

THE FUTURE OF GLOBAL TOMOGRAPHY: WAVEFORM TOMOGRAPHY

Most long wavelength tomographic models rely on phase and travel time data and therefore are restricted to phases (especially for body waves) that are well separated on seismograms. Furthermore, the use of ray theory prevents the utilization of

diffracted waves, whereas these phases provide critical sampling of the D″ region immediately above the CMB. Finally, the use of phase and travel time information only may not allow the resolution of small-scale low-velocity regions because of the "wavefront healing" effect (e.g., Nolet & Dahlen 2000, Wielandt 1987). This may be critical, for example, for better resolving the morphology of the lower mantle superplumes and their connection to surface hot spots. Moreover, the infinite frequency approximation used for body wave travel times restricts the sensitivity of a given phase to be uniformely distributed along the infinitesimal ray path. In order to more fully exploit information contained in the seismic wavefield, even at relatively long periods, broadband waveform inversion capabilities are required, and therein lies the future of global tomography.

The theoretical framework used for waveforms and surface wave phase velocities in present tomographic studies is generally that of zeroth order asymptotic theory for normal modes and surface waves [the path average approximation (PAVA), e.g., Woodhouse & Dziewonski 1984] in which it is assumed that sensitivity is confined to the great circle path between the epicenter and the station and varies along this path only with depth (1-D kernels). Physical insight on what is needed to compute "broadband" sensitivity kernels for body waves is obtained from the results of normal mode perturbation theory. In the zeroth order approximation (PAVA), asymptotic coupling along a single mode branch provides the ability to distinguish heterogeneity located on the minor and major arc (odd degree heterogeneity, e.g., Mochizuki 1986, Romanowicz 1987), but the corresponding kernels are 1-D, i.e., they vary uniformely with depth along the entire source-station path (Figure 9). In order to reproduce the variation of sensitivity along the ray path, across-branch coupling needs to be included (Li & Tanimoto 1993, Li & Romanowicz 1995, Marquering & Snieder 1995). To zeroth order in the asymptotic approximation,

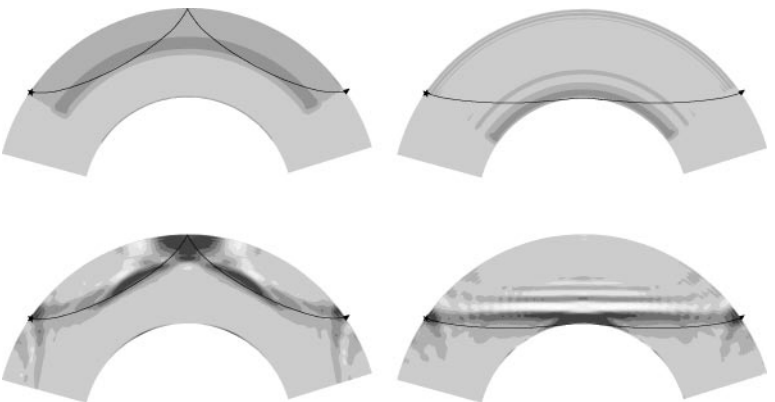

Figure 9 Comparison of sensitivity kernels for SS (*left*) and Sdiff (*right*), using the surface wave PAVA approximation (*top*) and the NACT approximation (*bottom*) (from Li & Romanowicz 1995).

this brings out some key features of body wave broadband sensitivity kernels, namely that the sensitivity is significant across some width around the ray (related to the Fresnel zone) depending on the frequency content of the waves considered, and also that it varies with position along the ray, being stronger near the source and receiver as well as around the location of surface bounce points and near the bottoming points of the ray (Figure 9).

To zeroth order in the asymptotic approximation, the kernels obtained are 2-D; that is, only the effects of structure in the vertical plane containing the source and the receiver are taken into account. To obtain 3-D kernels, which incorporate the effects of out of plane focusing, it is necessary to include higher-order terms in the asymptotic expansions (e.g., Romanowicz 1987), or to numerically compute integrals involving single scattering terms. Such theoretical first order 3-D kernels have been developed for seismic waveforms (Marquering et al. 1998) and for travel times (Dahlen et al. 2000, Zhao et al. 2000). Friederich (1999) has developed a formalism based on normal mode theory that allows the inclusion of multiple forward scattering terms. So far, however, 3-D kernels have not yet been fully implemented in global waveform tomography, mostly because of their heavy computational needs. This will no longer be an issue in the near future.

On the other hand, Li & Romanowicz (1995) have developed and applied a nonlinear asymptotic normal mode approach (NACT, nonlinear asymptotic coupling theory) in which global tomographic S velocity models are obtained by inverting waveform data exclusively, using 2-D asymptotic kernels as described above. Although off-great circle path propagation due to elastic effects has yet to be accounted for, this approach is the first step toward full waveform tomography and allows, in particular, the inclusion of S diffracted waveforms as well as wavepackets containing contributions from several phases that sample the mantle very differently (for example, ScS and SSS). The introduction of 2-D kernels (as opposed to PAVA) for higher-mode surface waves and body waveforms is particularly important for improving the resolution in the transition zone and mid-mantle (Mégnin & Romanowicz 1998). Because there is no "true" reference to compare with, it is not possible to assert at present, whether the differences in details seen among different tomographic models are related mostly to differences in datasets used, or also to the theoretical framework. For example, model SAW24B16 (Figure 8), which was constructed using 2-D kernels, shows a stronger continuation of the African plume toward the top of the lower mantle than other models. It is worth stressing that checkerboard tests, which are commonly used to assess the resolution of a given tomographic model, are only valid as long as the underlying wave propagation approximations are valid, but do not inform us on the "true" resolution, which would necessitate forward computations using an exact 3-D wave propagation code.

An issue in working with waveforms is that accurate knowledge of the earthquake source radiation is necessary. At relatively low frequencies (e.g., periods greater than 20 s), and if the dataset excludes the largest events, the point-source

approximation is sufficient, and an iterative scheme can be implemented to successively solve for 3-D structure and for source parameters.

OTHER PHYSICAL PARAMETERS DERIVED USING SEISMIC TOMOGRAPHY

Anisotropy in the Upper Mantle

It has been known since the 1970s that the uppermost mantle is anisotropic and that the strongest signal reflects transverse isotropy with $V_{sh} > V_{sv}$. Ignoring anisotropy has been shown to bias depth distribution of heterogeneity in V_s (e.g., Regan & Anderson 1984). This type of anisotropy has been taken into account in the spherically symmetric preliminary reference Earth model (PREM; Dziewonski & Anderson 1981), which includes transverse isotropy with vertical symmetry axis down to a depth of 220 km. Nataf et al. (1986) were the first ones to include transverse isotropy in their 3-D upper mantle V_s model based on surface wave phase velocity data and found a belt of $V_{sv} > V_{sh}$ around the Pacific following the ridge and subduction zone systems in the depth range of 200–400 km. Surface waves are also sensitive to variations in velocity as a function of azimuth due to more general orientation of anisotropy in the upper mantle (e.g., Montagner & Nataf 1986). Tanimoto & Anderson (1985) provided the first maps of azimuthal anisotropy in V_s at the global scale, showing that the fast axis of anisotropy aligns perpendicular to mid-ocean ridges, particularly around the East Pacific Rise, thus confirming that anisotropy reflects the dynamics of plate motions in the oceans. Montagner & Tanimoto (1990, 1991) developed a formalism that allowed them to invert for a more general model of anisotropy: transverse isotropy with a symmetry axis of variable orientation. In order to restrict the number of parameters in their model, they applied constraints based on mineralogy of olivine. They were thus able to obtain maps of isotropic V_s, the parameter $\xi = (V_{sh} - V_{sv})/V_{sv}$, which describes transverse isotropy, as well as azimuthal variations of anisotropy. Laske & Masters (1998) documented possible trade-offs in the resolution of azimuthal anisotropy and pointed out the potential usefulness of polarization data to help separate isotropic and anisotropic effects, as did Larson et al. (1998) . Babuśka et al. (1998) analyzed the variations of ξ under continents in the model of Montagner & Tanimoto (1991) and found systematic variations depending on the age of the lithosphere down to depths of 200–250 km, with $V_{sv} > V_{sh}$ under old shields and $V_{sh} > V_{sv}$ under Phanerozoic belts. On the other hand, Ekström & Dziewonski (1998) inverted three-component surface wave data for V_{sh} and V_{sv} distributions in the upper mantle and drew attention to the strong $V_{sh} > V_{sv}$ anomaly (in excess by 2% with respect to the PREM reference), down to a depth of 200 km, centered around Hawaii in the Pacific Ocean (Figure 10).

Anisotropy (at least transverse isotropy with a vertical symmetry axis) can no longer be ignored in tomographic inversions for upper mantle V_s structure, and is at least partly responsible for relatively poor correlation among current

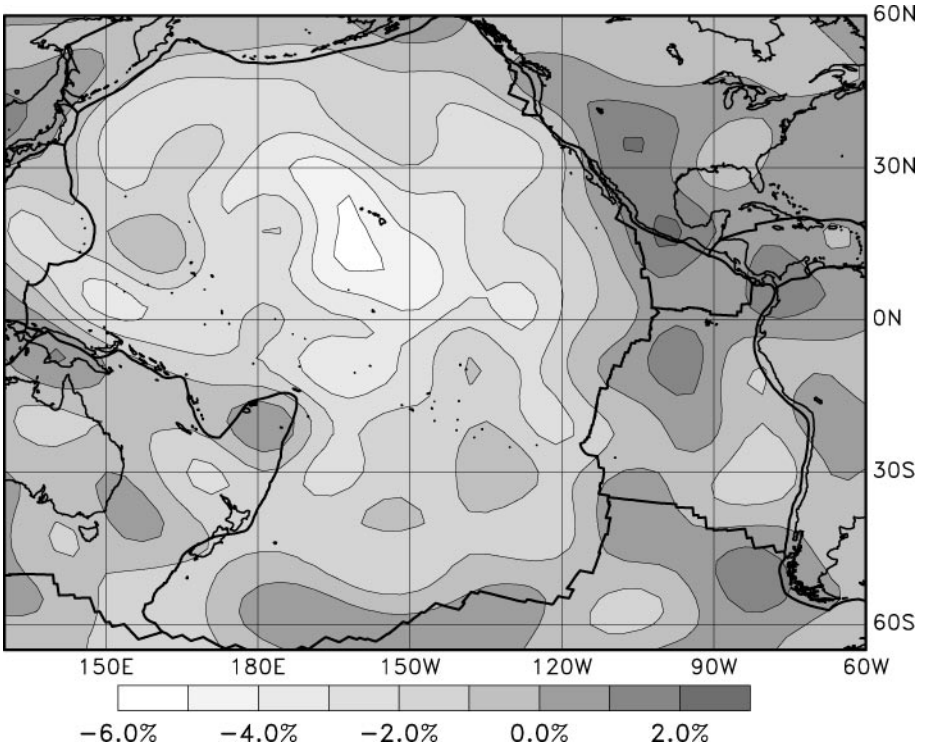

Figure 10 Variations in polarization anisotropy $(V_{sh} - V_{sv})/(V_{sh}$ in percent) at 150-km depth under the Pacific ocean in the model of Ekström & Dziewonski (1998). Courtesy of Göran Ekström.

isotropic models. Indeed, the datasets used by different groups have different sensitivity to the effect of anisotropy. For example, *S20RTS* (Ritsema et al. 1999) is constructed using Rayleigh waves (sensitive primarily to V_{sv}) to constrain upper mantle structure, whereas *SAW24B16* is based exclusively on transverse component waveform data (sensitive primarily to V_{sh}). Most other models use a combination of three-component data. The resulting differences can be clearly seen in Figure 6 at a depth of 140 km, especially in the central Pacific.

Attenuation in the Upper Mantle

Attenuation tomography has progressed more slowly than elastic tomography due to the difficulties of extracting anelastic signal from seismic wave amplitudes in the presence of significant elastic effects due to wave propagation in a heterogeneous Earth. So far, most attempts at extracting lateral variations in Q have been restricted to the upper mantle, except for a model by Bhattacharyya et al. (1996), which used body wave amplitude ratios in an attempt to resolve 3-D lateral

variations in Q in the whole mantle. Two recent reviews describe the issues involved in retrieving Q information in the mantle (Romanowicz 1998, Romanowicz & Durek 2000), and we only briefly summarize recent results. Durek et al. (1993) produced a very long wavelength even degree model (degrees 2, 4, and 6) of uppermost mantle attenuation, using amplitude ratios of consecutive Earth-circling Rayleigh wavetrains. Under the assumption that attenuation and elastic velocity are correlated as a function of depth, they found that lateral variations in attenuation may be mostly concentrated in the depth range of 100–300 km. Romanowicz (1995) obtained a degree 6–equivalent model of upper mantle attenuation using Rayleigh wave spectra in the period range of 100–320 s, and a methodology that allowed her to solve for odd-heterogeneity by removing tradeoffs with uncertainties in the source amplitude (Romanowicz 1994a). She found good correlation with tectonics in the Q distribution in the first 250 km of the upper mantle, and correlation with the hot spot distribution in the upper mantle transition zone (Romanowicz 1994b). Both Romanowicz (1995) and Durek et al. (1993) used a similar approach in order to desensitize Rayleigh wave amplitudes to elastic effects, using combinations of successive Earth-circling wavetrains and a linearized theoretical framework to describe elastic focusing effects and exploiting the fact that intrinsic attenuation is additive regardless of the direction of propagation, whereas elastic focusing effects change sign (to first order) depending on that direction.

These models (including Bhattacharyya et al. 1996) may be considered as "first generation" tomographic models of upper mantle attenuation and are primarily of qualitative value. More recently, several studies have produced somewhat better constrained second generation models using differential body wave phases (Reid et al. 2001, Warren & Shearer 2002), three-component-long period waveforms of fundamental and higher mode surface waves (Romanowicz & Gung 2002), or Rayleigh wave amplitudes (Billien & Lévêque 2000, Selby & Woodhouse 2002). The body wave studies have limited depth resolution but confirm the correlation of attenuation with tectonics at shallow mantle depth, as do the Rayleigh wave maps. Romanowicz & Gung (2002) developed an iterative waveform inversion procedure in which 3-D elastic structure is obtained in a first step, and once the waveform phases are matched with synthetics, the amplitude perturbations are inverted for a degree 8 Q model. Careful data selection is applied to reject waveforms strongly contaminated by focusing. Up to degree 8, as Selby & Woodhouse (2000) have shown, Q structure can be retrieved stably in the presence of realistic elastic effects. Model QRL8 (Romanowicz & Gung 2002) confirms once again correlation of Q with tectonics in the first 250 km of the upper mantle and with hot spots in the transition zone, where the correlation of Q distribution is also very strong with the distribution of V_s at the base of the mantle. Based on this model and elastic lower mantle models, Romanowicz & Gung (2002) have proposed that the two lower mantle superplumes, under Africa and the central Pacific, extend throughout the upper mantle to the base of the lithosphere. Figure 11 shows a comparison of recent Q models, illustrating some stable features correlated with tectonics.

Bulk Sound Velocity: Relation Between P and S Distributions in the Mantle

Comparisons of S and P tomographic models of the mantle should, in principle, provide information on the distribution of bulk sound velocity V_Φ as well as the depth (and lateral) distribution of the ratio $R = dlnV_s/dlnV_p$. When confronted with experimental results on mantle minerals, constraints on the thermal/compositional nature of heterogeneity in the deep mantle can thus be obtained. Results from direct comparison of V_s and V_p models have been questioned, however, because such models involve different sampling of the earth, different frequency ranges, and different damping constraints. In the past 10 years, several attempts at jointly inverting *P* and *S* datasets for common source-receiver pairs have been made. Several studies employed travel time data from the ISC bulletins (Vasco et al. 1995, Robertson & Woodhouse 1996, Vasco & Johnson 1998) and have confirmed the increase in R as a function of depth from $R \sim 1.7$ in the upper mantle to $R > 2.5$ in the lower mantle, in contradiction with mineral physics experiments as well as theoretical work that obtain maximum values of R 2.5, even when including anharmonic and pressure effects (e.g., Agnon & Bukowinski 1990, Karato 1993, Karato & Karki 2001). Su & Dziewonski (1997) used a combination of P-travel times from ISC and long-period S waveforms and travel times collected and measured individually. These authors inverted for V_s and bulk sound velocity V_Φ, which can more directly separate temperature and composition effects, and found significant anticorrelation between these two parameters in the deep mantle, especially at depths greater than 2000 km. Kennett et al. (1998) used ISC data for both *P* and *S* to also invert for V_s and V_Φ and found little correlation between these parameters in the lowermost mantle. This is also the depth range where Robertson & Woodhouse (1996) found that V_s and V_p are no longer well correlated. Masters et al. (2000) compared hand-picked $SS - S$ and $PP - P$ travel time residuals and confirmed their good correlation, and $R \sim 1.7$ in the upper mantle. On the other hand, when comparing *S* and *P* travel time residuals for different bottoming point depths, the strong increase with depth of R is again clear, with a maximum in D$''$ at $R \sim 3.8$.

Another type of joint inversion for V_s and V_p or V_s and V_Φ is possible from normal mode splitting data (e.g., Li et al. 1991). More recent studies have benefitted from a greatly expanded and higher quality mode dataset. Inversions for V_s and V_Φ (Masters et al. 2000, Ishii & Tromp 2001) find strong anticorrelation between these two parameters in the last 500 km of the mantle, confirming the results from body wave studies. Romanowicz (2001) inverted normal mode data for degree 2 structure and also found an increase of the ratio R in the lower mantle, reaching in excess of $R \sim 3$ at depths greater than 2000 km.

Whether travel time data or mode data are used, recent results confirm that R reaches values much in excess of $R = 2.5$ and that V_s is anticorrelated with V_Φ in the deep mantle, thus implying the necessity to invoke a contribution from lateral variations in chemistry, at least at depths greater than 2000 km. However, the lack

of correlation between V_s and V_p distributions in the lowermost mantle casts some doubt as to the validity of measuring R in this depth range.

Density

Whether or not lateral variations of density in the mantle, and particularly in the lowermost mantle, can be reliably resolved is a subject of active controversy. In principle, low angular order normal modes have some sensitivity to density. Taking advantage of the large collection of high-quality normal mode data accumulated over the past decade through the increase in the number of quiet global digital stations, and through the occurrence of several large deep earthquakes, in particular, the 06/09/1994 M8.2 deep Bolivia earthquake, Ishii & Tromp (1999, 2001) assembled a collection of mantle-sensitive normal mode splitting data and inverted them for even structure in V_s, bulk modulus (κ), and density (ρ) up to spherical harmonic degree 6 throughout the mantle. The shear and bulk-sound velocity distribution that they obtained is consistent with other models. On the other hand, their density model (SPRD6), the first published 3-D density model of the mantle, is poorly correlated with the velocity models. Its most striking feature is, in fact, anticorrelation of the ρ distribution with V_s in the D$''$ region, with high density associated with low velocity in the central Pacific and under Africa, which would imply a chemical contribution to lateral heterogeneity in the deep mantle, a result compatible with the partial decorrelation between V_s and V_p found in the same depth range and discussed above. However, this model poses some difficulties from the dynamic point of view, as it is not clear that it is possible to maintain high-density heterogeneity in a major upwelling such as the Pacific "superplume" (e.g., McNamara & van Keken 2000).

In fact, the robustness of these results has been questioned by several authors because the sensitivity of mantle free oscillations to density variations is rather weak. Resovsky & Ritzwoller (1999a,b) pointed out the ill-posed character of the inversion for density and showed that the model of density retrieved is very sensitive to initial constraints on the inversion. Romanowicz (2001) generated families of degree 2 models of density that fit the splitting data equally well but have opposite signs in the correlation with V_s in the lowermost mantle. Using a direct inversion method to obtain a 3-D Earth model using normal mode spectra, Kuo (2000) obtained a very different model of density from that of Ishii & Tromp (1999), which led Kuo & Romanowicz (2002) to perform extensive synthetic resolution tests. These authors found that the V_s and V_p heterogeneity can be independently resolved (at least to degree 6); however, lateral variations in density could be strongly contaminated by starting assumptions on the velocity models, and therefore not resolved, unless their amplitude is large enough (larger than 0.5%). There are, however, no reliable constraints at this point on the possible lateral variations of density in the lowermost mantle.

Presently, the question of lateral variations in density in the mantle remains open and is still a challenge for future tomographers.

Topography of the 660-km Discontinuity

Some important geophysical questions that are still the subject of debate concern the nature of the 660-km discontinuity and its role in the global circulation. It is generally assumed that it corresponds to an olivine phase change (e.g., Ringwood 1969), but it has also been suggested that a compositional change may occur around that depth (e.g., Irifune 1998). Lateral variations in thickness of the transition zone and their correlation with volumetric velocity variations may shed some light on this question.

In order to retrieve fine-scale information about the thickness and topography of upper mantle discontinuities, it is necessary to study relatively short period body waves that interact with these discontinuities through reflections or conversions. Different mapping techniques have been developed for this purpose.

Although numerous studies have been conducted at the regional scale, two main techniques have been applied to study transition zone discontinuities on the global scale, albeit with very uneven sampling around the globe. The first one is based on the observation of precursors to surface reflections, such as PP, SS, or P′P′ (e.g., Shearer & Masters 1992; Shearer 1993; Gossler & Kind 1996; Eastabrook & Kind 1996; Flanaghan & Shearer 1998, 1999; Gu et al. 1998; Gu & Dziewonski 2002). The second one is based on the observation of phases converted at discontinuities, such as Pds (Chevrot et al. 1999). Both approaches involve stacking procedures to enhance the weak signal associated with discontinuity structure. Although techniques based on precursors allow a better global distribution of sampling points, they have the drawback of being associated with minimax phases, which has raised the issue of possible contamination by small-scale, off-great circle path structure (e.g., Neele et al. 1997, Shearer et al. 1999). On the other hand, converted phases, which are minimum travel time phases, allow better resolution, in principle, due to their smaller Fresnel zones, but the global sampling is poorer. Also, the spatial averaging kernel of precursors may allow more robust estimates of long wavelength structure.

There are some first-order differences between results obtained using converted versus reflected phases. SS precursor studies agree on the existence of large ($\sim$40 km) lateral variations in the thickness of the transition zone, as measured using differences between travel times of reflections off the 410-km and 660-km discontinuities. These measurements should be independent of the complexity of structure in the crust and uppermost mantle, and therefore are thought to represent the transition zone thickness rather well. The lateral variations seem to be mostly due to topography on the 660 km discontinuity. There is correlation with volumetric lateral variations of velocity in the transition zone from tomographic studies. A generally consistent feature is the increased thickness of the transition zone associated with subducted slabs in the western Pacific and under South America (Figure 12), in agreement with what is predicted for cold regions due to the negative Clapeyron slope of the phase change associated with that discontinuity, and a reduced thickness under the central Pacific ocean, also in agreement with temperature effects on phase changes. However, some studies find a correlation of spatial variations of topography and transition zone thickness with ocean and

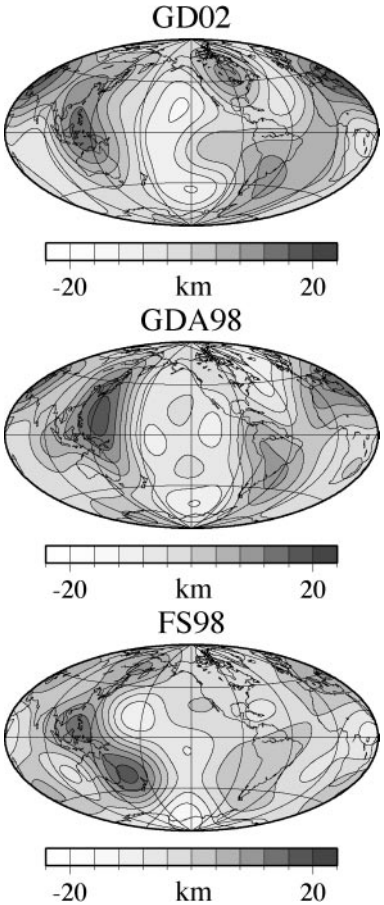

Figure 12 Topography of the 670-km discontinuity obtained using precursors to SS in three recent studies: FS98 (Flanaghan & Shearer 1998), GDA98 (Gu et al. 1998), and GD02 (Gu & Dziewonski 2002). Courtesy of Yu Gu.

continent distribution (Gossler & Kind 1996, Gu et al. 1998), whereas others don't (e.g., Flanagan & Shearer 1998, 1999).

Chevrot et al. (1999) complemented an existing dataset of Sdp travel time measurements (Stammler et al. 1992) using stacking techniques at stations of the global seismic networks and found very small (less than 10 km) global variations in the thickness of the transition zone. On the other hand, the converted phase travel times correlate very strongly with the tectonic setting (i.e., the uppermost mantle structure) of the station considered. However, more recent work by Lebedev et al. (2002) at the regional scale (south-Western Pacific) using converted phases seems to indicate a correlation of transition zone thickness with volumetric velocity, in agreement with the phase transition interpretation, indicating a possible reconciliation of results obtained using precursor versus converted phases.

DISCUSSION AND CONCLUSIONS

Current global V_p tomographic models based on the ISC dataset provide good insight into the variety of behaviors of subducted slabs as they descend into the lower mantle, even though their exact connection with high-velocity structure near the core mantle boundary is still not clear. On the other hand, V_s tomographic models, based on recently accumulated broadband data, provide constraints on the longest wavelength structure as well as on the morphology of low-velocity regions associated with rising currents. Images of the latter are not as sharp as those of the subduction zones, in part because of the theoretical issue tied to the use of travel times of seismic phases, and in part because of a data coverage problem.

The development of an improved theoretical framework, coupled with more powerful computers, has opened the way to waveform tomography and the possibility of exploiting more fully the richness of broadband seismograms. However, major efforts to instrument the ocean floor with long-term broadband seismic observatories must also continue, as vast areas of the globe, especially in the southern oceans, remain poorly covered.

In addition, forward modeling of travel times indicates that large lateral variations of structure, in excess of $\pm 5\%$ occur at the base of the mantle on lengths scales of a few hundred kilometers, at least in the vicinity of the two large "superplumes" (e.g., Ritsema et al. 1998, Bréger & Romanowicz 1998, Ni & Helmberger 1999, Ni et al. 2002).

Such strong variations, as well as those known to occur in the crust and uppermost mantle, have so far been beyond the reach of tomography, in particular, due to the limitations of the theoretical framework employed; ray theory does not handle diffraction and frequency dependence, whereas normal mode perturbation theory requires weak and smooth lateral variations of structure. However, we are currently reaching a turning point in seismology, where beyond forward modeling of travel times, it is becoming practical to compute full synthetic seismograms in a global spherical geometry as opposed to cartesian Earth, in as complex 3-D structures as necessary, and down to periods of interest (10 s or less), using numerical methods based on the use of spectral elements (e.g., Komatitch & Vilotte 1998, Komatitch & Tromp 1999, Capdeville et al. 2003). These computations can provide valuable insights and better physical understanding on the interaction between heterogeneity and seismic wave propagation as expressed in observed waveforms and an assessment of the appropriate level of approximation that is sufficient for tomographic modeling. This should lead to theoretical improvements that will enable tomographers to take into account the key effects at affordable computational costs.

Clearly, the full level of understanding of the complexity of structure in Earth's mantle and in particular at its base, will only be achieved by a combination of precise forward modeling and tomographic inversion approaches, and sustained efforts in global observations, particularly in the oceans.

ACKNOWLEDGMENTS

The author wishes to thank Y. Fukao, Y. Gu, G. Ekström, L. Warren, D. Vasco, and R. van der Hilst for allowing her to include figures from their work in this paper. She also thanks Y.C. Gung and Y. Gu for helping with figure preparation.

The *Annual Review of Earth and Planetary Science* is online at http://earth.annualreviews.org

LITERATURE CITED

Agnon A, Bukowinski M. 1990. δ_s at high pressure and $dlnV_s/dlnV_p$ in the lower mantle. *Geophys. Res. Lett.* 17:1149–52

Aki K, Christofferson A, Husebye E. 1977. Determination of the three-dimensional structure of the lithosphere. *J. Geophys. Res.* 82: 277–96

Albarède F, van der Hilst RD. 1999. New mantle convection model may reconcile conflicting evidence. *EOS Trans. Am. Geophys. Union* 80:535–39

Babuśka V, Montagner JP, Plomerova J, Girardin N. 1998. Age-dependent large-scale fabric of the mantle lithosphere as derived from surface wave velocity anisotropy. *Pure Appl. Geophys.* 121:257–80

Bhattacharyya J, Masters G, Shearer P. 1996. Global lateral variations of shear wave attenuation in the upper mantle. *J. Geophys. Res.* 101:22,273–89

Bijwaard H, Spakman W. 1999. Tomographic evidence for a narrow whole mantle plume below Iceland. *Earth Planet. Sci. Lett.* 166: 121–26

Bijwaard H, Spakman W, Engdahl ER. 1998. Closing the gap between regional and global travel time tomography. *J. Geophys. Res.* 103:30,055–78

Billien M, Lévêque JJ. 2000. Global maps of Rayleigh wave attenuation for periods between 40 and 150 seconds. *Geophys. Res. Lett.* 27:3619–22

Boschi L, Dziewonski AM. 1999. High and low-resolution images of the Earth's mantle: implications of different approaches to tomographic modeling. *J. Geophys. Res.* 104: 25,567–94

Boschi L, Dziewonski AM. 2000. Whole Earth tomography from delay times of *P*, *PcP*, and *PKP* phases: lateral heterogeneities in the outer core or radial anisotropy in the mantle? *J. Geophys. Res.* 105:13,675–96

Boschi L, Ekström G. 2002, New images of the Earth's upper mantle from measurements of surface-wave phase velocity anomalies. *J. Geophys. Res.* 10.1029/2000JB000059

Bréger L, Romanowicz B. 1998. Thermal and chemical 3D heterogeneity in D″. *Science:* 282:718–20

Bullen K. 1963. *Introduction to the Theory of Seismology*. New York: Cambridge Univ. Press. 381 pp.

Capdeville Y, Chaljub E, Vilotte JP, Montagner JP. 2003. Coupling the spectral element method with a modal solution for elastic wave propagation in global Earth models. *Geophys. J. Int.* 152:34–67

Chiao LY, Kuo BY. 2001. Multiscale seismic tomography. *Geophys. J. Int.* 145:517–27

Chevrot S, Vinnik L, Montagner JP. 1999. Global scale analysis of the mantle Pds phases. *J. Geophys. Res.* 104:20,203–19

Creager K, Jordan TH. 1986. Aspherical structure of the core-mantle boundary from PKP travel times. *Geophys. Res. Lett.* 13:1497–500

Dahlen FA, Hung SH, Nolet G. 2000. Fréchet kernels for finite-frequency travel times—I. Theory. *Geophys. J. Int.* 141:157–74

Doornbos D, Hilton T. 1989. Models of core-mantle boundary and the travel times of internally reflected core phases. *J. Geophys. Res.* 94:15,741–51

Durek JJ, Ritzwoller MH, Woodhouse JH. 1993. Constraining upper mantle anelasticity using surface wave amplitudes. *Geophys. J. Int.* 114:249–72

Dziewonski AM. 1984. Mapping the lower mantle: determination of lateral heterogeneity in P velocity up to degree and order 6. *J. Geophys. Res.* 89:5929–52

Dziewonski AM, Anderson DL. 1981. Preliminary reference Earth model. *Phys. Earth Planet. Int.* 25:297–356

Dziewonski AM, Hager BH, O'Connell RJ. 1977. Large scale heterogeneities in the lower mantle. *J. Geophys. Res.* 82:239–55

Ekström G, Dziewonski AM. 1998. The unique anisotropy of the Pacific upper mantle. *Nature* 394:168–72

Ekström G, Tromp J, Larson EW. 1997. Measurements and models of global surface wave propagation. *J. Geophys. Res.* 102:8137–57

Engdahl ER, van der Hilst RD, Buland RP. 1998. Global teleseismic earthquake relocation with improved travel times and procedures for depth determination. *Bull. Seismol. Soc. Am.* 88:722–43

Estabrook CH, Kind R. 1996. The nature of the 660-km upper-mantle seismic discontinuity from precursors to the PP phase. *Science* 274:1179–82

Flanaghan MP, Shearer PM. 1998. Global mapping of topography on transition zone velocity discontinuities by stacking SS precursors. *J. Geophys. Res.* 103:2673–92

Flanagan MP, Shearer PM. 1999. A map of topography on the 410-km discontinuity from PP precursors. *Geophys. Res. Lett.* 26:549–52

Foulger G, Pritchard M, Julian B, Evans J. 2000. The seismic anomaly beneath Iceland extends down to the mantle transition zone and no deeper. *Geophys. J. Int.* 142:F1–5

Friederich W. 1999. Propagation of seismic shear and surface waves in a laterally heterogeneous mantle by multiple forward scattering. *Geophys. J. Int.* 136:180–204

Fukao Y, Widiyantoro S, Obayashi M. 2001. Stagnant slabs in the upper and lower mantle transition region. *Rev. Geophys.* 39:291–323

Garnero EJ. 2000. Heterogeneity of the lowermost mantle. *Annu. Rev. Earth Planet. Sci.* 28:509–37

Garnero EJ, Helmberger DV. 1996. Seismic detection of a thin laterally varying boundary layer at the base of the mantle beneath the central-pacific. *Geophys. Res. Lett.* 23:977–80

Gossler J, Kind R. 1996. Seismic evidence for very deep roots of continents. *Earth Planet. Sci. Lett.* 138:1–13

Grand SP. 1994. Mantle shear structure beneath the Americas and surrounding oceans. *J. Geophys. Res.* 99:11,591–621

Grand SP. 2002. Mantle shear wave tomography and the fate of subducted slabs. *Phil. Trans. R. Soc. London.* In press

Grand SP, van der Hilst R, Widiyantoro S. 1997. Global seismic tomography: a snapshot of convection in the Earth. *GSA Today* 7(4):1–7

Gung YC, Romanowicz B. 2002. Q tomography of the upper mantle using three component long period waveforms. *J. Geophys. Res.* In press

Gu YJ, Dziewonski AM. 2002. Global variability of transition zone thickness. *J. Geophys. Res.* 10.1029/2001JB000489

Gu YJ, Dziewonski AM, Agee CB. 1998. Global decorrelation of the topography of transition zone discontinuities. *Earth Planet. Sci. Lett.* 157:57–67

Gu YJ, Dziewonski AM, Su WJ, Ekström G. 2001. Models of the mantle shear velocity and discontinuities in the pattern of lateral heterogeneities. *J. Geophys. Res.* 106: 11169–199

Hung SH, Dahlen FA, Nolet G. 2000. Fréchet kernels for finite-frequency travel times—II. Examples. *Geophys. J. Int.* 141:175–203

Irifune T, Nishiyama N, Kuroda K, Inoue T, Isshike M, et al. 1998. The postspinel phase boundary in Mg (sub 2) SiO (sub 4) determined by in situ X-ray diffraction. *Science* 279:1698–70

Ishii M, Tromp J. 1999. Normal-mode and free-air gravity constraints on lateral variations in velocity and density of the Earth's mantle. *Science* 285:1231–36

Ishii M, Tromp J. 2001. Even-degree lateral variations in the Earth's mantle constrained by free oscillations and the free-air gravity anomaly. *Geophys. J. Int.* 145:77–96

Kamiya S, Miyatake T, Hirahara K. 1988. How deep can we see the high-velocity anomalies beneath the Japan Islands? *Geophys. Res. Lett.* 15:828–31

Karason H, van der Hilst RD. 2001. Improving global tomography models of P-wavespeed I: incorporation of differential travel times for refracted and diffracted core phases (PKP,Pdiff). *J. Geophys. Res.* 106:6569–87

Karato S. 1993. Importance of anelasticity in the interpretation of seismic tomography. *Geophys. Res. Lett.* 20:1623–26

Karato S, Karki B. 2001. Origin of lateral heterogeneity of seismic wave velocities and density in Earth's deep mantle. *J. Geophys. Res.* 106:21771–83

Kennett BLN, Widiyantoro S, van der Hilst RD. 1998. Joint seismic tomography for bulk sound and shear wave speed in the Earth's mantle. *J. Geophys. Res.* 103:12,469–93

Komatitsch D, Vilotte JP. 1998. The spectral element method: an effective tool to simulate the seismic response of 2D and 3D geological structures. *Bull. Seism. Soc. Am.* 88:368–92

Komatitsch D, Tromp J. 1999, Introduction to the spectral element method for three-dimensional seismic wave propagation. *Geophys. J. Int.* 139:806–22

Kuo BY, Garnero EJ, Lay T. 2000. Tomographic inversion of S-SKS times for shear velocity heterogeneity in D″; degree 12 and hybrid models. *J. Geophys. Res.* 105:28,139–57

Kuo C. 2000. *Three-dimensional density structure of the Earth: limits to astrophysical and seismological approaches*. PhD thesis, Univ. Calif. Berkeley. 177 pp.

Kuo C, Romanowicz B. 2002. On the resolution of density anomalies in the Earth's mantle using spectral fitting of normal mode data. *Geophys. J. Int.* 150:162–79

Larson EWF, Tromp J, Ekström G. 1998. Effects of slight anisotropy on surface waves. *Geophys. J. Int.* 132:654–66

Laske G, Masters G. 1996. Constraints on global phase velocity maps by long-period polarization data. *J. Geophys. Res.* 101: 16,059–75

Laske G, Masters G. 1998. Surface wave polarization data and global anisotropic structure. *Geophys. J. Int.* 132:508–20

Lavely EM, Rodgers A, Ritzwoller MH. 1994. Can the differential sensitivity of body wave, mantle wave, and normal mode data resolve the trade-off between transition zone structure and boundary topography? *Phys. Earth Planet. Inter.* 86:117–46

Lebedev S, Chevrot S, van der Hilst R. 2002. Seismic evidence for olivine phase changes at the 410- and 660-kilometer discontinuities. *Science* 296:1300–2

Li XD, Tanimoto T. 1993. Waveforms of long period body waves in a slightly aspherical Earth. *Geophys. J. Int.* 112:92–112

Li XD, Romanowicz B. 1995. Comparison of global waveform inversions with and without considering cross branch coupling. *Geophys. J. Int.* 121:695–709

Li XD, Romanowicz B. 1996. Global mantle shear velocity model developed using nonlinear asymptotic coupling theory. *J. Geophys. Res.* 101:22,245–73

Li XD, Giardini D, Woodhouse JH. 1991. The relative amplitudes of mantle heterogeneity in P-velocity, S-velocity and density from free-oscillation data. *Geophys. J. Int.* 105: 649–57

Liu XF, Dziewonski AM. 1998. Global analysis of shear wave velocity anomalies in the lowermost mantle. In *The Core-Mantle Boundary Region*, ed. M Gurnis, N Wysession, E Knittle, B Buffett, 28:21–36. Washington, DC: Am. Geophys. Union

Marquering H, Snieder R. 1995. Surface-wave mode coupling for efficient forward modelling and inversion of body wave phases. *Geophys. J. Int.* 120:186–208

Marquering H, Nolet G, Dahlen FA. 1998. Three-dimensional waveform sensitivity kernels. *Geophys. J. Int.* 124:258–78

Masters G, Johnson S, Laske G, Bolton H. 1996. A shear-velocity model of the mantle. *Philos. Trans. R. Soc. London A* 354:1385–411

Masters G, Laske G, Bolton H, Dziewonski AM. 2000. The relative behavior of shear velocity, bulk sound speed, and compressional velocity in the mantle: implications for chemical and thermal structure. In *Earth's Deep Interior: Mineral Physics and Tomography from the Atomic to the Global Scale*, ed. S Karato, AM Forte, RC Liebermann, G Masters, L Stixrude, 117:63–87. Washington, DC: Am. Geophys. Union

McNamara AK, van Keken PE. 2000. Cooling of the Earth: a parameterized convection study of whole vs. layered models. *Geochem. Geophys. Geosys.* 1:15 (November 2000)

Mégnin C, Romanowicz B. 1998. The effect of theoretical formalism and data selection scheme on mantle models derived from waveform tomography. *Geophys. J. Int.* 138: 366–80

Mégnin C, Romanowicz B. 2000. The 3D shear velocity structure of the mantle from the inversion of body, surface and higher mode waveforms. *Geophys. J. Int.* 143:709–28

Mochizuki E. 1986. Free oscillations and surface waves in an aspherical earth. *Geophys. Res. Lett.* 13:1478–81

Montagner JP. 1986. Regional three-dimensional structures using long-period surface waves. *Ann. Geophys.* 4:283–94

Montagner JP, Nataf HC. 1986. A simple method for inverting the azimuthal anisotropy of surface waves. *J. Geophys. Res.* 91: 511–20

Montagner JP, Tanimoto T. 1990. Global anisotropy in the upper mantle inferred from the regionalization of phase velocities. *J. Geophys. Res.* 95:4797–819

Montagner JP, Tanimoto T. 1991. Global upper mantle tomography of seismic velocities and anisotropy. *J. Geophys. Res.* 96:20,337–51

Mooney WD, Laske G, Masters G. 1998. CRUST-5.1: a global crustal model at $5^o \times 5^o$. *J. Geophys. Res.* 103:727–47

Morelli A, Dziewonski AM. 1987. Topography of the core-mantle boundary and lateral homogeneity of the liquid core. *Nature* 325:678–83

Nataf HC, Nakanishi I, Anderson DL. 1986. Measurements of mantle wave velocities and inversion for lateral heterogeneities and anisotropy. Part III: inversion. *J. Geophys. Res.* 91:7261–307

Nataf HC, Ricard Y. 1996. 3SMAC: an a priori tomographic model of the upper mantle based on geophysical modeling. *Phys. Earth. Planet. Int.* 95:101–22

Neele F, de Regt H, VanDecar J. 1997. Gross errors in upper-mantle discontinuity topography from underside reflection data. *Geophys. J. Int.* 129:194–204

Ni S, Helmberger DV. 1999. Low-velocity structure beneath Africa from forward modeling. *Earth Planet. Sci. Lett.* 170:497–507

Ni S, Tan E, Gurnis M, Helmberger DV. 2002. Sharp sides to the African Superplume. *Science* 296:1850–52

Nolet G. 1990. Partitioned waveform inversion and two-dimensional structure under the network of autonomously recording seismographs. *J. Geophys. Res.* 95:8499–512

Nolet G, Dahlen FA. 2000. Wave front healing and the evolution of seismic delay times. *J. Geophys. Res.* 105:19,043–54

Obayashi M, Fukao Y. 1997. P and PcP travel time tomography for the core-mantle boundary. *J. Geophys. Res.* 102:17,825–41

Paige CC, Saunders MA. 1982. LSQR: an algorithm for sparse linear equations and sparse least squares. *ACM Trans. Math. Software* 8:43–71

Regan J, Anderson DL. 1984. Anisotropic models of the uppermantle. *Phys. Earth Planet. Int.* 35:227–63

Reid FJL, Woodhouse JH, van Heist HH. 2001. Upper mantle attenuation and velocity structure from measurements of differential S phases. *Geophys. J. Int.* 145:615–30

Resovsky JS, Ritzwoller MH. 1999a. A degree 8 mantle shear velocity model from normal mode observations below 3 mHz. *J. Geophys. Res.* 104:993–1014

Resovsky JS, Ritzwoller MH. 1999b. Regularization uncertainty in density models estimated from normal mode data. *Geophys. Res. Lett.* 26:2319–22

Ringwood AE. 1969. Phase transformations in

the mantle. *Earth Planet. Sci. Lett.* 5:401–12

Ritsema J, Ni S, Helmberger DV, Crotwell HP. 1998. Evidence for strong shear velocity reductions and velocity gradients in the lower mantle beneath Africa. *Geophys. Res. Lett.* 25:4245–48

Ritsema J, van Heijst HH, Woodhouse JH. 1999. Complex shear wave velocity structure imaged beneath Africa and Iceland. *Science* 286:1925–28

Ritzwoller MH, Lavely EM. 1995. Three-dimensional seismic models of the Earth's mantle. *Rev. Geophys.* 33:1–66

Robertson GS, Woodhouse JH. 1996. Ratio of relative S to P velocity heterogeneity in the lower mantle. *J. Geophys. Res.* 101:20,041–52

Rodgers A, Wahr J. 1993. Inference of core-mantle boundary topography from ISC PcP and PKP traveltimes. *Geophys. J. Int.* 115:991–1011

Romanowicz B. 1987. Multiplet-multiplet coupling due to lateral heterogeneity: asymptotic effects on the amplitude and frequency of the earth's normal modes. *Geophys. J. R. Astro. Soc.* 90:75–100

Romanowicz B. 1991. Seismic tomography of the Earth's mantle. *Annu. Rev. Earth Planet. Sci.* 19:77–99

Romanowicz B. 1994a. On the measurement of anelastic attenuation using amplitudes of low-frequency surface waves. *Phys. Earth Planet. Int.* 84:179–91

Romanowicz B. 1994b. Anelastic tomography: a new perspective on upper-mantle thermal structure. *Earth Planet. Sci. Lett.* 128:113–21

Romanowicz B. 1995. A global tomographic model of shear attenuation in the upper mantle. *J. Geophys. Res.* 100:12,375–94

Romanowicz B. 1998. Attenuation tomography of the Earth's mantle: a review of current status. *Pure Appl. Geophys.* 153:257–72

Romanowicz B, Durek J. 2000. Seismological constraints on attenuation in the earth: a review. *Geophys. Monogr.* 117:161–80

Romanowicz B. 2001. Can we resolve 3D density heterogeneity in the lower mantle? *Geophys. Res. Lett.* 28:1107–10

Romanowicz B, Gung YC. 2002. Mega-upwellings from the core-mantle boundary to the lithosphere: implications for heat flux. *Science* 296:513–16

Russell SA, Lay T, Garnero EJ. 1998. Seismic evidence for small-scale dynamics in the lowermost mantle at the root of the Hawaiian hotspot. *Nature* 396:255–58

Selby ND, Woodhouse JH. 2000. Controls on Rayleigh wave amplitudes: attenuation and focusing. *Geophys. J. Int.* 142:933–40

Selby ND, Woodhouse JH. 2002. The Q structure of the upper mantle: constraints from Rayleigh wave amplitudes. *J. Geophys. Res.* 107:933–40

Sengupta MK, Toksöz MN. 1977. Three-dimensional model of seismic velocity variation in the Earth's mantle. *Geophys. Res. Lett.* 3:84–86

Shearer PM, Masters G. 1992. Global mapping of topography on the 660 km discontinuity. *Nature* 355:791–96

Shearer PM. 1993. Global mapping of upper mantle reflectors from long-period SS precursors. *Geophys. J. Int.* 115:878–904

Shearer PM, Flanaghan M, Hedlin M. 1999. Experiments in migration processing of SS precursor data to image upper mantle discontinuity structure. *J. Geophys. Res.* 104:7229–42

Spakman W, Nolet G. 1988. Imaging algorithms: accuracy and resolution in delay time tomography. In *Mathematical Geophysics: A Survey of Recent Developments in Seismology and Geodynamics*, ed. NJ Vlaar, G Nolet, M Wortel, S Cloetingh, pp. 155–88, Dordrecht: D Reidel

Stammler K, Kind R, Petersen N, Kosarev G, Vinnik L, Qiyuan L. 1992. The upper mantle discontinuities: correlated or anti-correlated? *Geophys. Res. Lett.* 19:1563–66

Stark PB, Hengartner NW. 1993. Reproducing Earth's kernel: uncertainty of the shape of the core-mantle boundary from PKP and PcP travel times. *J. Geophys. Res.* 98:1957–71

Stevenson DJ. 1987. Limits on lateral density and velocity variations in the Earth's outer core. *Geophys. J. R. Astron. Soc.* 88:311–19

Su WJ, Dziewonski AM. 1997. Simultaneous inversion for 3-D variations in shear and bulk velocity in the mantle. *Phys. Earth Planet. Int.* 100:135–56

Su WJ, Woodward RL, Dziewonski AM. 1994. Degree 12 model of shear velocity heterogeneity in the mantle. *J. Geophys. Res.* 99: 4945–80

Sylvander M, Souriau A. 1996. P-velocity structure of the core-mantle boundary region inferred from PKP(AB)-PKP(BC) differential travel times. *Geophys. Res. Lett.* 23:853–56

Tanimoto T. 1997. Global images of the upper 200 km in the Earth by short-period surface waves. *J. Phys. Earth* 45:203–26

Tanimoto T, Anderson DL. 1985. Lateral heterogeneity and azimuthal anisotropy of the upper mantle: Love and Rayleigh waves 100–250 s. *J. Geophys. Res.* 90:1842–58

Tkalčić H, Romanowicz B, Houy N. 2002. Constraints on D′′ structure using PKP(AB-DF), PKP(BC-DF) and PcP-P travel time data from broadband records. *Geophys. J. Int.* 149:599–616

Trampert J, Woodhouse JH. 1996. High resolution global phase velocity distributions. *Geophys. Res. Lett.* 23:21–24

van der Hilst R, Spakman W. 1989. Importance of the reference model in linearized tomography and images of the subduction below the Caribbean plate. *Geophys. Res. Lett.* 16:1093–96

van der Hilst R, Karason H. 1999. Compositional heterogeneity in the bottom 1000 kilometers of Earth's mantle: towards a hybrid convection model. *Science* 283:1885–88

van der Hilst R, Widiyantoro S, Engdahl E. 1997. Evidence for deep mantle circulation from global tomography. *Nature* 386:578–84

Vasco DW, Johnson LR. 1998. Whole Earth structure estimated from seismic arrival times. *J. Geophys. Res.* 103:2633–71

Vasco DW, Johnson LR, Pulliam J. 1995. Lateral variations in mantle velocity structure and discontinuities determined from *P*, *PP*, *S*, *SS* and $SS - S_dS$ travel time residuals. *J. Geophys. Res.* 100:24,037–59

Vinnik L, Bréger L, Romanowicz B. 1998. Anisotropic structures at the base of the mantle. *Nature* 393:564–67

Wang Z, Dahlen FA. 1995. Spherical-spline parametrization of three-dimensional Earth models. *Geophys. Res. Lett.* 22:3099–102

Warren LM, Shearer PM. 2002. Mapping lateral variation in upper mantle attenuation by stacking *P* and *PP* spectra. *J. Geophys. Res.* 10.1029/2001JB01195

Wielandt E. 1987. On the validity of the ray approximation for interpreting delay times. In *Seismic Tomography; With Applications to Global Seismology and Exploration Geophysics*, ed. G Nolet, pp. 85–98. Dordrecht: D Reidel

Woodhouse JH, Dziewonski AM. 1984. Mapping the upper mantle: three-dimensional modeling of Earth structure by inversion of seismic waveforms. *J. Geophys. Res.* 89: 5953–86

Zhang YS, Tanimoto T. 1993. High-resolution global upper mantle structure and plate tectonics. *J. Geophys. Res.* 98:9793–823

Zhang YS, Lay T. 1996. Global surface wave phase velocity variations. *J. Geophys. Res.* 101:8415–36

Zhao L, Jordan TH, Chapman C. 2000. Three-dimensional Fréchet differential kernels for seismic delay times. *Geophys. J. Int.* 141: 558–76

Zhou HW. 1996. A high resolution P wave model for the top 1200 km of the mantle. *J. Geophys. Res.* 101:27,791–810

Zhao D. 2001. Seismic structure and origin of hotspots and mantle plumes. *Earth Planet. Sci. Lett.* 192:251–65

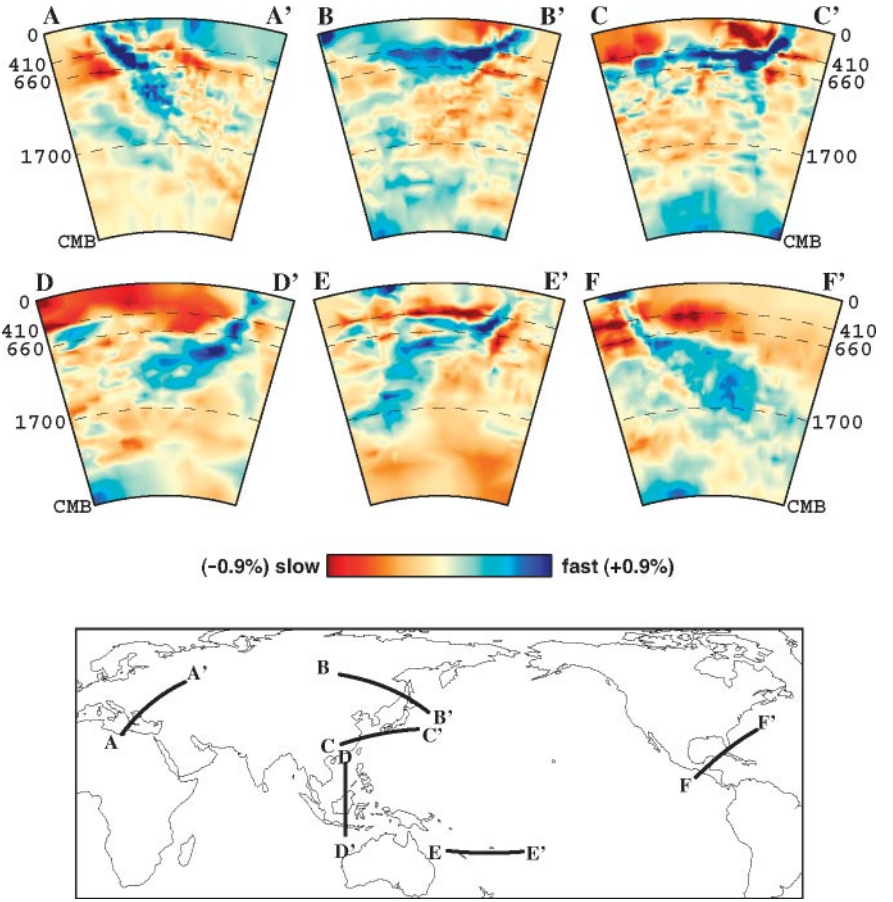

Figure 2 Examples of depth cross sections in several subduction zone areas showing fast anomalies associated with subducted slabs as revealed by P travel time tomography using ISC data (from Karason & van der Hilst 2000).

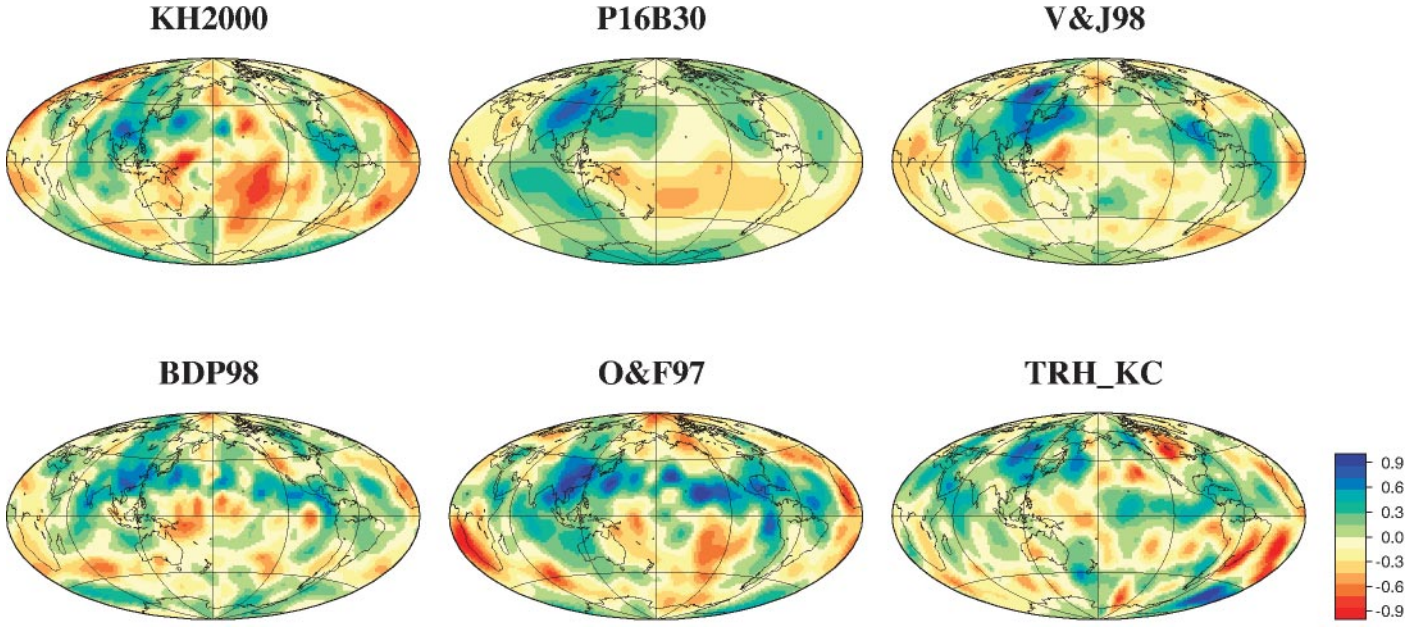

Figure 3 Comparison of P velocity models at a depth of 2800 km: KH2000 (Karason & van der Hilst 2000); P16B30 (Masters et al. 2000); VJ98 (Vasco & Johnson 1998); BDP98 (Bijwaard et al. 1999); OF97 (Obayashi & Fukao 1997); TRH_{kc} (Tkalčić et al. 2002). The scale is in percent of average P velocity at this depth.

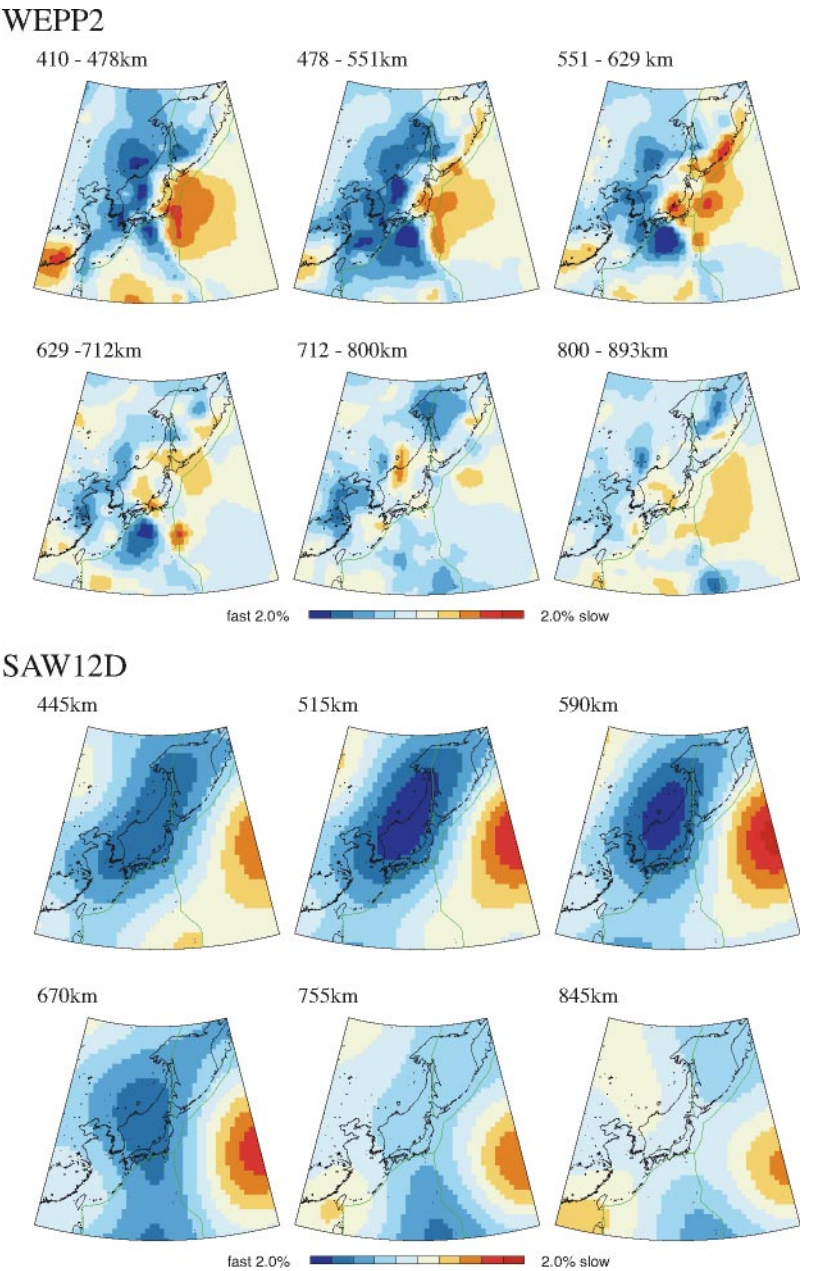

Figure 7 Maps of the subduction zone areas around Japan at different depths in the transition zone showing lateral variations in velocity obtained in a "high resolution" P velocity model [*top*, WEPP2 (Obayashi et al. 1997)] compared to those obtained in a "long wavelength" S model [*bottom*, SAW12D (Li & Romanowicz 1996)].

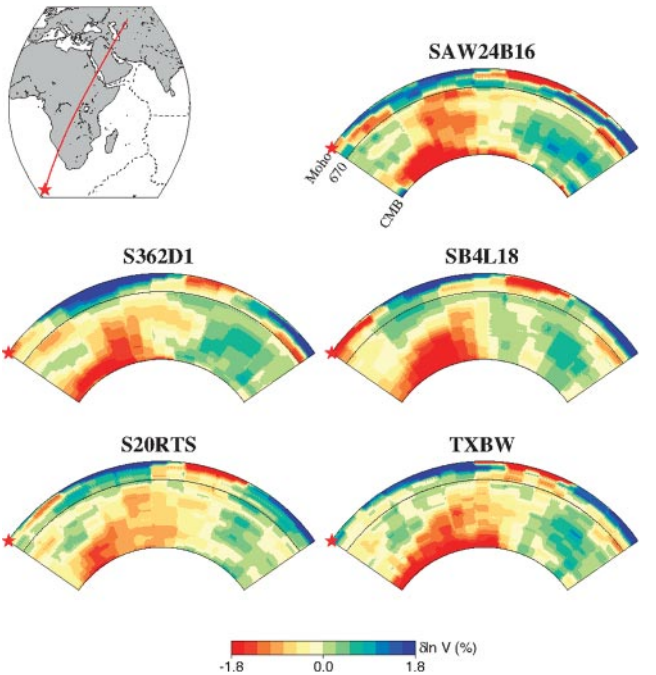

Figure 8 Comparison of cross sections across the African "superplume" for the five S velocity models displayed in Figure 6.

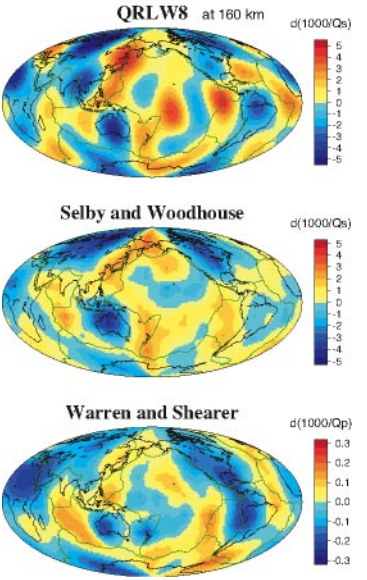

Figure 11 Lateral variations in Q of the upper mantle obtained by different approaches. (*Top*) variations in shear attenuation (Q_β^{-1}) at a depth of 160 km obtained using surface waveforms by Romanowicz & Gung (2002). (*Middle*) variations in Q_β^{-1} in the top 250 km of the mantle, using amplitude ratios of S and SS waves (Selby & Woodhouse 2001). (*Bottom*) average variations in Q_α^{-1} in the top 250 km of the mantle, obtained using amplitude ratios of P and PP waves (Warren & Shearer 2002).

Annual Review of Earth and Planetary Sciences
Volume 31, 2003

CONTENTS